Letter

Field orientation dependent magnetic phases in the Weyl semimetal $Co_3Sn_2S_2$

Samuel E. Pate,[1,2] Bin Wang,[3] Bing Shen,[3] J. Samuel Jiang,[1] Ulrich Welp,[1] Wai-Kwong Kwok,[1] Jing Xu,[4] Kezhen Li,[1,2] Ralu Divan,[4] and Zhi-Li Xiao[1,2,*]

[1]*Materials Science Division, Argonne National Laboratory, Argonne, Illinois 60439, USA*
[2]*Department of Physics, Northern Illinois University, DeKalb, Illinois 60115, USA*
[3]*School of Physics, Sun Yat-sen University, Guangzhou 510275, China*
[4]*Center for Nanoscale Materials, Argonne National Laboratory, Argonne, Illinois 60439, USA*

(Received 3 August 2023; accepted 18 September 2023; published 29 September 2023)

Magnetism plays a key role in the emergence of topological phenomena in the Weyl semimetal $Co_3Sn_2S_2$, which exhibits ferromagnetic interactions along the *c*-axis of the crystal and antiferromagnetic (AFM) interactions within the *ab* plane. Extensive studies on the temperature dependence of the magnetism with the magnetic field along the *c*-axis have uncovered a number of magnetic phases. Currently, the nature and origins of the reported magnetic phases are under debate. Here we report on magnetic field orientation effects on the magnetism in $Co_3Sn_2S_2$. The shape of the hysteresis loop of the Hall resistance at a fixed temperature is found to change from rectangular to bow tie-like as the magnetic field is tilted from the *c*-axis toward the *ab* plane, resembling that reported for magnetic fields along the *c*-axis as the temperature approaches the Curie temperature from below. Unlike their temperature-dependent counterparts, the newly observed bow tie-like hysteresis loops show exchange bias. Our results showcase the contribution of the in-plane AFM interactions to the magnetism in $Co_3Sn_2S_2$ and demonstrate a new way to tune its magnetic phases. They also shed light on the temperature-dependent magnetic phases occurring in the magnetic field along the *c*-axis of the crystal.

DOI: 10.1103/PhysRevB.108.L100408

Recently, $Co_3Sn_2S_2$ was discovered to be a Weyl semimetal [1–4] with topologically nontrivial behavior such as a giant anomalous Hall effect [1,2] and Hall angle [1,5], chiral anomaly-induced negative magnetoresistance [1], large magneto-optical response [6], and a strong spin polarization [7,8]. It exhibits magnetic order below the Curie temperature T_C [1,2,6], arising from the *d* orbitals of cobalt ions arranged in a kagome lattice in the *ab* plane [9]. First-principle calculations [10] reveal ferromagnetism (FM) with cobalt magnetic moments aligned parallel to the *c*-axis. Experiments at low temperatures confirm that the *c*-axis of the crystal is the easy axis of magnetization and a field of $H = 23$ T is required to orient the cobalt magnetic moment parallel to the kagome plane fully at $T = 2$ K [11].

As the first confirmed, intrinsic time-reversal symmetry-breaking Weyl semimetal, $Co_3Sn_2S_2$ has launched extensive investigations on its magnetic order [12–27], which is strongly correlated with the band structure and topological semimetallic states [14–16,19,28,29], leading to the discovery of intriguing magnetic phases [12–15,18–20,22–27]. For example, temperature-dependent ac magnetic susceptibility measurements uncovered an anomalous magnetic phase (denoted as A-phase) at low fields near T_C [12,19]. High-resolution muon spin-rotation (μSR) experiments indicate that $Co_3Sn_2S_2$ crystals exhibit a *c*-axis FM ground state at low temperatures. When the temperature is increased toward T_C, the volume of the FM component is found to decrease while an in-plane antiferromagnetic (AFM) phase emerges and becomes dominant at temperatures near T_C. The magnetic competition between these two phases is found to be highly tunable by applying pressure [13,14] or doping [21,22]. New magnetic phases have also been suggested from the measurements on the magnetic field dependence of the magnetization $M(H)$ and anomalous Hall effect $R_{xy}(H)$, where a change from a rectangular to a bow tie-like structure of the $M(H)$ and $R_{xy}(H)$ hysteresis loops was observed and attributed to a freezing transition of the spin glass state arising from the strong magnetic frustration in the *ab* plane [15].

Currently, experiments revealing possible magnetic phases focus on thermal effects, with magnetic fields applied along the *c*-axis of the crystal. Although extensive investigations have been conducted, the nature and origins of these possible magnetic phases, particularly the contribution of the in-plane AFM structures, have been widely debated [14–29]. In this Letter, we investigate the effects of magnetic field orientation on magnetic phases by tilting the magnetic field from the *c*-axis toward the *ab* plane. We measure $R_{xy}(H)$ hysteresis loops at a fixed temperature while changing the direction of the magnetic field. We find that the shape of the hysteresis loops can change from rectangular to bow tie-like when the magnetic field is rotated from the *c*-axis toward the *ab* plane. Remarkably, this behavior is similar to that observed for magnetic field along the *c*-axis [15] when the temperature is increased toward T_C. The shape variation in the $R_{xy}(H)$ hysteresis loops driven by the magnetic field orientation is observed at temperatures down to the lowest experimentally available temperature ($T = 3$ K), while occurring only at a

*xiao@anl.gov or zxiao@niu.edu

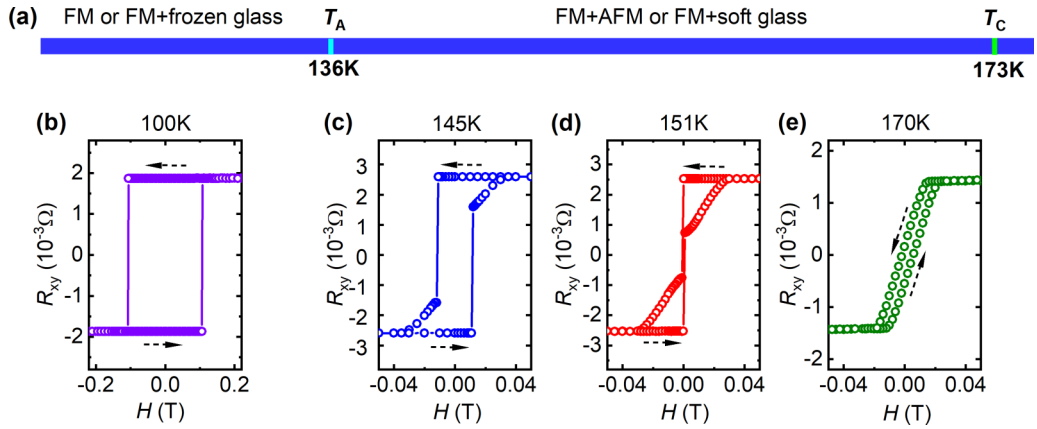

FIG. 1. (a) Horizontal blue bar indicates a temperature T_A separating various magnetic phases, with FM at $T < T_A$ and FM + AFM at $T > T_A$ revealed in μSR measurements in Ref. [14] as well as FM + frozen glass at $T < T_A$ and FM + soft glass at $T > T_A$ suggested in Ref. [15] from the shapes of $M(H)$ and $R_{xy}(H)$ hysteresis loops. (b)–(e) Representative $R_{xy}(H)$ hysteresis loops obtained at $T = 100$ K, 145 K, 151 K, and 170 K, respectively. The magnetic field was orientated along the c-axis. The sample has $T_C = 173$ K (see Supplemental Material Fig. S2 [30]) and $T_A = 136$ K (see Supplemental Material Fig. S3 [30]). The dashed arrows indicate the sweeping directions of the magnetic field.

temperature-insensitive and narrow angle range (<6°) from the *ab* plane. Together with the accompanying exchange bias, the bow tie-like $R_{xy}(H)$ hysteresis loops observed in the vicinity of the *ab* plane highlight the role of AFM interaction in the magnetism in $Co_3Sn_2S_2$. Our results also provide evidence for the contribution of the AFM structure to the appearance of previously reported temperature-dependent magnetic phases and demonstrate a new way to tune the magnetic phases of this Weyl semimetal.

Our measurements were conducted on two crystals grown by a self-flux method [1]. They show consistent results and data presented here are from one of them. The $R_{xy}(H)$ hysteresis loops were obtained using the Electrical Transport Option of a Quantum Design PPMS. Electrical leads were gold wires arranged in a Hall bar geometry, glued to the crystal using silver epoxy H20E. A low-frequency (21.36-Hz) ac current of 1 mA was applied in the *ab* plane and the angular dependencies of the resistance were obtained by placing the sample on a precision stepper-controlled rotator with an angular resolution of 0.005°. The magnetic field was rotated in the plane perpendicular to the current. The magnetic field orientation is represented by θ, which is defined as the angle between the applied magnetic field and the c-axis. Experimentally, the orientation of the *ab* plane with respect to the magnetic field is determined by measuring the angle dependence of the Hall resistance R_{xy} at $H = \pm 7$ T. The crossing point of the two curves for $H = \pm 7$ T is defined as $\theta = 90°$, corresponding to $\mathbf{H}||ab$. To avoid contribution of the magnetic moment to the anisotropy of R_{xy}, we conducted measurements in the paramagnetic state, i.e., at $T = 300$ K, and the results are presented in Supplemental Material Fig. S1 [30].

As indicated by the resistance-versus-temperature curve presented in Supplemental Material Fig. S2 [30] for zero-field cooling, our crystal has a Curie temperature of $T_C \approx 173$ K, consistent with those in the literature, ranging from $T_C \approx 172$ K to 177 K [1,2,9,14–17]. Figure 1 shows the $R_{xy}(H)$ loops obtained at various temperatures for magnetic fields aligned along the c-axis, which exhibit similar temperature-induced shape changes as those reported in the literature [15]. More specifically, the loop at $T = 100$ K is rectangular with binary switchable magnetic moments, reflecting collective spin flips, while the loops at $T = 145$ K and 151 K show bow tie-like structures, as termed in Ref. [15], with the former exhibiting "triangular tails" and the latter showing "double triangles." More detailed measurements allowed us to identify a temperature of $T_A \approx 136$ K (see Supplemental Material Fig. S3 and its caption [30]) that clearly separates regimes where $R_{xy}(H)$ loops are rectangular (at $T < T_A$) and bow tie-like (at $T > T_A$). This value of T_A is nearly the same as those ($T_A = 135$ K [12] and ≈130 K [19]) at which an anomaly occurs in the magnetic susceptibility. Moreover, it is about 10 K higher than the spin glass freezing temperature of $T_G \approx 125$ K [15]. In reported studies, the temperature above which anomalous magnetic phases were observed varies between 125 K and 135 K [6,12,18,19,23–26].

The bow tie-like structure of the hysteresis loops in $Co_3Sn_2S_2$ at $T > T_A$ was understood as the interplay of two terms in the free energy in a minimal Landau model, one favoring a FM structure $M = \pm M_0$, and another favoring in-plane AFM structures $M = 0$ [15]. In other words, hysteresis loops with a bow tie-like structure indicate the coexistence of the out-of-plane FM order with an in-plane AFM structure. Due to the absence of exchange bias (EB) expected for a mixed phase of FM and AFM orders, it was hypothesized [15] that the in-plane AFM structure is a soft or dynamic spin glass arising from the magnetic frustration in the kagome lattice, which coexists but does not interact with the FM structure. With decreasing temperature, the spin glass becomes frozen, leading to the occurrence of EB observed in the sample at $T < T_A$. That is, T_A is the glass freezing transition temperature (thus was denoted T_G in Ref. [15]).

Since the AFM structure was also detected in μSR measurements at $T > T_A$ [14], the previous understanding [15] seems to be plausible. Indeed, $M(H)$ hysteresis loops with very similar bow tie-like structures as those reported in Ref. [15]

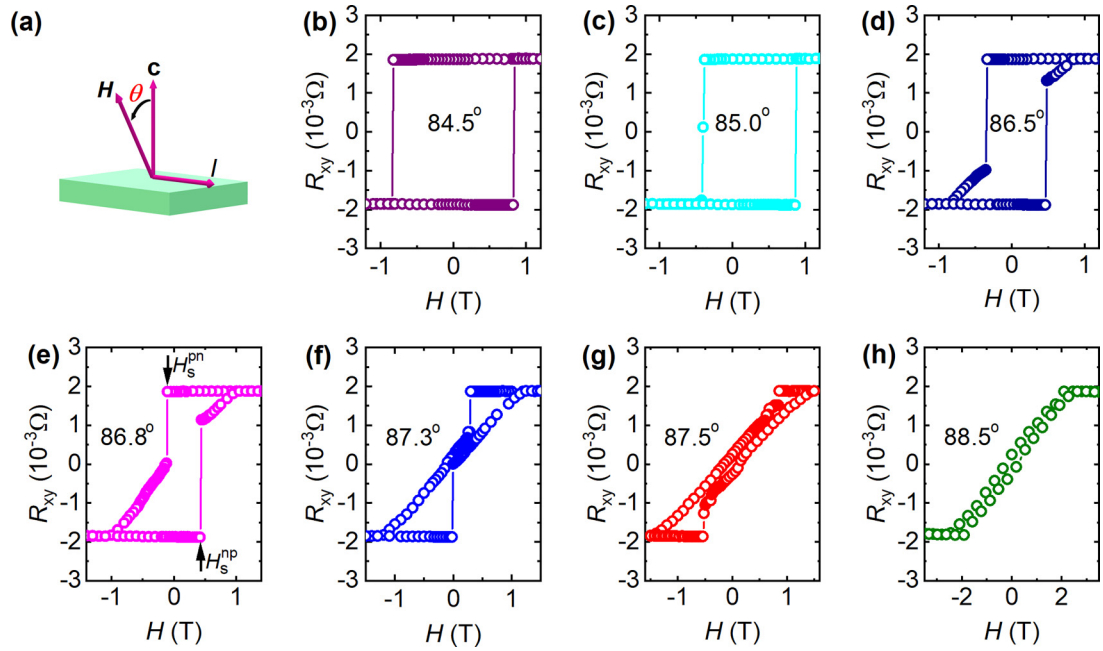

FIG. 2. (a) Schematic of the magnetic field orientation, where θ is the angle between the applied magnetic field and the crystal's c-axis. (b)–(h) Representative $R_{xy}(H)$ hysteresis loops obtained at $\theta = 84.5°$, 85.0°, 86.5°, 86.8°, 87.3°, 87.5°, and 88.5°, respectively. The data were obtained at $T = 100$ K with the magnetic field rotation plane perpendicular to the current flow direction. The definitions of H_s^{pn} and H_s^{np} are given in (e).

and resembling our $R_{xy}(H)$ loops in Fig. 1 were also observed in rare-earth orthoferrites [31–34], in which FM and AFM structures can coexist and the expected EB often does not occur either [32,34]. However, the bow tie-like hysteresis loops without EB in rare-earth orthoferrites were explained by a reversible motion of a single magnetic domain wall in the sample, i.e., without involving the mixture of FM and AFM orders [32]. Furthermore, "double triangles" were observed in hysteresis loops of materials without an AFM structure [35,36]. Thus, further evidence is desirable to support the current understanding of the observed bow tie-like structures in the hysteresis loops of $Co_3Sn_2S_2$.

Our key findings are displayed in Fig. 2, which presents $R_{xy}(H)$ loops at $T < T_A$ and for magnetic fields oriented close to the ab plane. It demonstrates that $R_{xy}(H)$ loops can exhibit bow tie-like structures at $T < T_A$ with concurrent EB, implying that antiferromagnetism may indeed contribute to the bow tie-like structures in the $R_{xy}(H)$ loops at $T > T_A$, regardless of the EB's absence due to the temperature-induced softening of the AFM structure. Since T (=100 K)< T_A (=136 K), the $R_{xy}(H)$ loop is expected to be rectangular for $\boldsymbol{H} \parallel c$, i.e., at $\theta = 0°$, as shown in Fig. 1(b). The rectangular shape stays unchanged even at an angle as large as $\theta = 84.5°$ [Fig. 2(b)]. However, a small tail occurs at the negative field side of the $R_{xy}(H)$ loop at $\theta = 85.0°$ [Fig. 2(c)]. When the magnetic field is further tilted toward the ab plane, triangular tails appear on both sides of the loops, as exhibited by those at $\theta = 86.5°$ [Fig. 2(d)] and 86.8° [Fig. 2(e)], followed by hysteresis loops with double triangles, as shown in Figs. 2(f) and 2(g) for $\theta = 87.3°$ and $\theta = 87.5°$, respectively. The bow tie-like structures eventually vanish when the magnetic field is within about 2° of the ab plane [see Fig. 2(h) for $\theta = 88.5°$]. That is, magnetic phases similar to those observed at $\boldsymbol{H} \parallel c$ and $T > T_A$ (Fig. 1 and Ref. [15]) can occur at a fixed temperature $T < T_A$ as the magnetic field tilts toward the ab plane. Furthermore, unlike those for $\boldsymbol{H} \parallel c$ and $T > T_A$, the $R_{xy}(H)$ loops with bow tie-like structures in Figs. 2(c)–2(g) are asymmetric with respect to the zero field, i.e., the loops are exchange biased.

The evolution of the shape of the $R_{xy}(H)$ loops with the magnetic field orientation is further illustrated by the angle dependence of the switching fields, as presented in Fig. 3. The switching fields H_s^{np} and H_s^{pn} are the values of the magnetic field prior to the abrupt changes in R_{xy} when the magnetic field is swept from negative to positive and from positive to negative, respectively, as denoted in Fig. 2(e). At $\theta \leqslant 82.5°$, H_s^{pn} and H_s^{np} monotonically increase as the magnetic field tilts away from the c-axis toward the ab plane while having the same values but with opposite signs [Fig. 3(a)], i.e., $|H_{ss}^{pn}| = H_s^{pn}$, reflecting the symmetry of the $R_{xy}(H)$ loops with respect to the zero field. At larger angles [see Fig. 3(b) for an expanded view], the values of H_s^{pn} and H_s^{np} fluctuate, and in most cases are not equal, indicating possible exchange bias. In particular, they start to decrease with increasing angle after a small tail occurs at the negative field side of the $R_{xy}(H)$ loop [at $\theta > 85.0°$, Fig. 2(c)]. In a very narrow-angle regime ($87° < \theta < 88°$) associated with the occurrence of the double triangles in the $R_{xy}(H)$ loops [Figs. 2(f) and 2(g)], H_s^{pn} and H_s^{np} change their signs and their values also increase rapidly.

Exchange bias is typically parameterized as $H_{EB} = (H_{+C} + H_{-C})/2$, where H_{+C} and H_{-C} represent the coercive fields for the positive and negative fields, respectively, reflecting that the loop is centered around a nonzero-field H_{EB} instead of $H = 0$ T [15,37]. While it works well for rectangular loops, such a definition of H_{EB} does not appropriately reflect the asymmetry in the hysteresis loops with bow tie-like structures [see Figs. 2(e) and 2(f)]. In our analysis, we

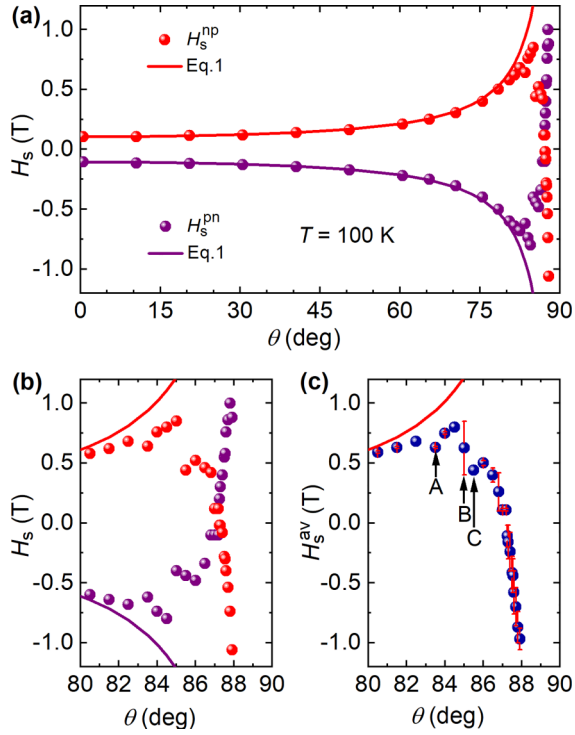

FIG. 3. (a) Angle dependence of the switching fields H_s^{pn} and H_s^{np} [defined in Fig. 2(e)]. Symbols and lines represent experimental data and fits from Eq. (1), respectively. (b) Expanded view of the data in (a) for the magnetic field oriented in the vicinity of the *ab* plane. (c) Angle dependence of the averaged switching field $H_s^{av} = (H_s^{np} - H_s^{pn})/2$ and the exchange bias $H_{EB} = (H_s^{np} + H_s^{pn})/2$, which are presented as solid symbols and error bars, respectively. Letters A, B and C denote the three angles at which the measurements were repeated twice for comparison, and the data are presented in Supplemental Material Fig. S6 [30].

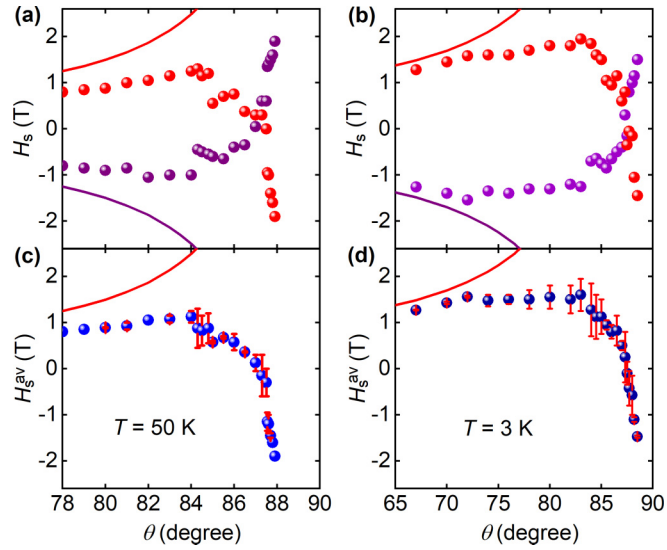

FIG. 4. (a) and (b) Angle dependence of the switching fields H_s^{pn} (purple symbols) and H_s^{np} (red symbols) for $T = 50$ K and 3 K, respectively. Symbols and lines represent experimental data and fits from Eq. (1), respectively. (c) and (d) Angle dependence of the averaged switching field $H_s^{av} = (H_s^{np} - H_s^{pn})/2$ and the exchange bias $H_{EB} = (H_s^{np} + H_s^{pn})/2$, which are presented as blue symbols and red error bars, respectively. For clarity, we present only data in the angle regime where EB and bow tie-like structures in the hysteresis loops are observed. Complete data sets of H_s^{pn} and H_s^{np} are presented in Supplemental Material Fig. S5 [30].

replace H_{+C} and H_{-C} with H_s^{np} and H_s^{pn}, respectively, i.e., $H_{EB} = (H_s^{np} + H_s^{pn})/2$, which is equivalent to the conventional definition when the loops are rectangular. Figure 3(c) exhibits the angle dependence of H_{EB} as error bars to the averaged switching field $H_s^{av} = (H_s^{np} - H_s^{pn})/2$. It shows that the loops with double triangles always have significant EBs, while those with "triangle tails" can sometimes be symmetric, i.e., $H_{EB} = 0$. Interestingly, the largest EBs seem to occur at the transitions separating regimes where the loops are rectangular, with triangular tails and double triangles, respectively. While the values of H_s^{np} and H_s^{pn} in Fig. 3(b) and H_s^{av} in Fig. 3(c) obtained at $83^\circ < \theta < 86.5^\circ$ look to be random, the corresponding loops are highly reproducible, as demonstrated in Supplemental Material Fig. S4 [30], which presents comparisons of two measurement runs for loops obtained at three particular angles [denoted by A, B, C in Fig. 3(c)] where the H_s^{av} unexpectedly deviates from the overall increasing trend, the EB is the largest, and the H_s^{av} deviates from the overall decreasing trend, respectively.

The switching of spins in an ordinary ferromagnet is often caused by nucleation and motion of domain walls separating regions of opposite uniform magnetizations. The values of the associated switching fields depend on the angle θ between the magnetic field and the magnetization easy axis, following the Kondorsky relation [38–40]:

$$H_s(\theta) = H_s(0^\circ)/\cos\theta. \quad (1)$$

As presented in Fig. 3 as solid lines, Eq. (1) describes H_s^{np} and H_s^{pn} as well as H_s^{av} very well for θ up to $\sim 80^\circ$ while deviating from the experimental data as the magnetic field enters the angle regime where $R_{xy}(H)$ loops show EB and bow tie-like structures. Nearly the same behavior occurs at a lower temperature, $T = 50$ K, as demonstrated in Fig. 4(a) and (c), as well as Supplemental Material Fig. S5 [30]. At our lowest experimentally accessible temperature, $T = 3$ K, EB can be more unambiguously identified in a wider angle range [Figs. 4(b) and 4(d)]. However, this extension of the EB angle range arises from the exchange-biased rectangular loops (see Supplemental Material Fig. S6 [30]), while the angle regime $(84^\circ < \theta < 88^\circ)$ for the occurrence of bow tie-like structures seems to be temperature insensitive, as demonstrated by the large EB values at θ between 84° and 85° at all three temperatures.

Following the explanation proposed in Ref. [15] and discussed here on the origin of the bow tie-like structures, it seems reasonable to interpret the deviation from Eq. (1) as a transition from a pure FM state to a mixture of FM/AFM phases, since a magnetic field in the vicinity of the *ab* plane should suppress the *c*-axis FM interaction while enhancing the in-plane AFM interaction. Recent neutron scattering experiments [25] reveal that AFM structures at $T > T_A$ probably originate from a temperature-induced local lattice instability due to geometrical frustration in the cobalt kagome lattice. It is rational to hypothesize that such a local lattice instability

can be enhanced by a magnetic field not parallel to the *c*-axis since a nonzero torque exerting on the cobalt ions can distort the cobalt kagome lattice, thereby lowering the temperature at which AFM structures can exist. With increasing θ, the torque becomes larger, resulting in stronger local lattice instability. Thus, tilting the magnetic field toward the *ab* plane at a fixed temperature can lead to similar effects as the temperature approaches T_C at $\boldsymbol{H} \parallel c$ on magnetic phases.

In summary, we investigated magnetic field orientation effects on the magnetism in the newly confirmed ferromagnetic Weyl semimetal $Co_3Sn_2S_2$. We found that tilting the magnetic field from the *c*-axis toward the *ab* plane at a fixed temperature can induce a change in the magnetic phases similar to what occurs when the temperature is swept up to the Curie temperature while keeping the magnetic field aligned along the *c*-axis, as referred from the change (from rectangle to bow tie-like structure) in the shape of the $R_{xy}(H)$ hysteresis loops. Furthermore, the bow tie-like $R_{xy}(H)$ hysteresis loops observed near the *ab* plane can exhibit exchange bias, underscoring the significance of the AFM interaction for the magnetism in $Co_3Sn_2S_2$. Our results demonstrate a new way to tune the magnetic phases of $Co_3Sn_2S_2$ and shed light on the origin of the bow tie-like structures in the hysteresis loops measured in the magnetic field along the *c*-axis.

We thank Vitalii Vlasko-Vlasov for stimulating discussions. Experimental design and transport measurements were supported by the U.S. Department of Energy, Office of Science, Basic Energy Sciences, Materials Sciences and Engineering. S.E.P and Z.-L.X acknowledge support from the National Science Foundation (Grant No. DMR-1901843). B.W. and B.S. were supported by the National Natural Science Foundation of China (Grant No. U213010013), Natural Science Foundation of Guangdong Province (Grant No. 2022A1515010035), Guangzhou, Basic and Applied Basic Research Foundation (Grant No. 202201011798), and the open research fund of Songshan Lake Materials Laboratory (Grant No. 2021SLABFN11). Use of the Center for Nanoscale Materials, an Office of Science user facility, was supported by the U.S. Department of Energy, Office of Science, Office of Basic Energy Sciences (Contract No. DE-AC02-06CH11357).

[1] E. Liu *et al.*, Nat. Phys. **14**, 1125 (2018).
[2] Q. Wang, Y. Xu, R. Lou, Z. Liu, M. Li, Y. Huang, D. Shen, H. Weng, S. Wang, and H. Lei, Nat. Commun. **9**, 3681 (2018).
[3] D. F. Liu, A. J. Liang, E. K. Liu, Q. N. Xu, Y. W. Li, C. Chen, D. Pei, W. J. Shi, S. K. Mo, P. Dudin, T. Kim, C. Cacho, G. Li, Y. Sun, L. X. Yang, Z. K. Liu, S. S. P. Parkin, C. Felser, and Y. L. Chen, Science **365**, 1282 (2019).
[4] N. Morali, R. Batabyal, P. K. Nag, E. Liu, Q. Xu, Yan Sun, B. Yan, C. Felser, N. Avraham, and H. Beidenkopf, Science **365**, 1286 (2019).
[5] J. Shen, Q. Zeng, S. Zhang, H. Sun, Q. Yao, X. Xi, W. Wang, G. Wu, B. Shen, Q. Liu, and E. Liu, Adv. Funct. Mater. **30**, 2000830 (2020).
[6] Y. Okamura, S. Minami, Y. Kato, Y. Fujishiro, Y. Kaneko, J. Ikeda, J. Muramoto, R. Kaneko, K. Ueda, V. Kocsis, N. Kanazawa, Y. Taguchi, T. Koretsune, K. Fujiwara, A. Tsukazaki, R. Arita, Y. Tokura, and Y. Takahashi, Nat. Commun. **11**, 4619 (2020).
[7] H. Wang, Y. Liu, H. Zhou, H. Ji, J. Luo, J. Zhang, T. Wei, P. Wang, S. Jia, and J. Wang, Sci. China Phys. Mech. Astron. **63**, 287411 (2020).
[8] S. Howlader, S. Saha, R. Kumar, V. Nagpal, S. Patnaik, T. Das, and G. Sheet, Phys. Rev. B **102**, 104434 (2020).
[9] W. Schnelle, A. Leithe-Jasper, H. Rosner, F. M. Schappacher, R. Pottgen, F. Pielnhofer, and R. Weihrich, Phys. Rev. B **88**, 144404 (2013).
[10] Q. Xu, E. Liu, W. Shi, L. Muechler, J. Gayles, C. Felser, and Y. Sun, Phys. Rev. B **97**, 235416 (2018).
[11] J. Shen, Q. Zeng, S. Zhang, W. Tong, L. Ling, C. Xi, Z. Wang, E. Liu, W. Wang, G. Wu, and B. Shen, Appl. Phys. Lett. **115**, 212403 (2019).
[12] M. A. Kassem, Y. Tabata, T. Waki, and H. Nakamura, Phys. Rev. B **96**, 014429 (2017).
[13] X. Chen, M. Wang, C. Gu, S. Wang, Y. Zhou, C. An, Y. Zhou, B. Zhang, C. Chen, Y. Yuan, M. Qi, L. Zhang, H. Zhou, J. Zhou, Y. Yao, and Z. Yang, Phys. Rev. B **100**, 165145 (2019).
[14] Z. Guguchia *et al.*, Nat. Commun. **11**, 559 (2020).
[15] E. Lachman, R. A. Murphy, N. Maksimovic, R. Kealhofer, S. Haley, R. D. McDonald, J. R. Long, and J. G. Analytis, Nat. Commun. **11**, 560 (2020).
[16] R. Yang, T. Zhang, L. Zhou, Y. Dai, Z. Liao, H. Weng, and X. Qiu, Phys. Rev. Lett. **124**, 077403 (2020).
[17] M. A. Kassem, Y. Tabata, T. Waki, and H. Nakamura, J. Phys. Condens. Matter **33**, 015801 (2020).
[18] H. C. Wu, P. J. Sun, D. J. Hsieh, H. J. Chen, D. C. Kakarla, L. Z. Deng, C. W. Chu, and H. D. Yang, Mater. Today Phys. **12**, 100189 (2020).
[19] Q. Zhang, S. Okamoto, G. D. Samolyuk, M. B. Stone, A. I. Kolesnikov, R. Xue, J. Yan, M. A. McGuire, D. Mandrus, and D. A. Tennant, Phys. Rev. Lett. **127**, 117201 (2021).
[20] S. Howlader, R. Ramachandran, S. Y. Singh, and G. Sheet, J. Phys. Condens. Matter **33**, 075801 (2021).
[21] D. H. Shin, J. H. Jun, S. E. Lee, and M. H. Jung, arXiv:2105.03892.
[22] Z. Guguchia, H. Zhou, C. N. Wang, J.- X. Yin, C. Mielke III, S. S. Tsirkin, I. Belopolski, S.- S. Zhang, T. A. Cochran, T. Neupert, R. Khasanov, A. Amato, S. Jia, M. Z. Hasan, and H. Luetkens, npj Quantum Mater. **6**, 50 (2021).
[23] J. R. Soh, C. Yi, I. Zivkovic, N. Qureshi, A. Stunault, B. Ouladdiaf, J. A. Rodríguez-Velamazán, Y. Shi, H. M. Rønnow, and A. T. Boothroyd, Phys. Rev. B **105**, 094435 (2022).
[24] C. Lee, P. Vir, K. Manna, C. Shekhar, J. E. Moore, M. A. Kastner, C. Felser, and J. Orenstein, Nat. Commun. **13**, 3000 (2022).
[25] Q. Zhang, Y. Zhang, M. Matsuda, V. O. Garlea, J. Yan, M. A. McGuire, D. A. Tennant, and S. Okamoto, J. Am. Chem. Soc. **144**, 14339 (2022).

[26] I. Živković, J.- R. Soh, R. Yadav, C. Yi, Y. Shi, O. V. Yazyev, and H. M. Rønnow, Phys. Rev. B **106**, L180403 (2022).
[27] Z. Shen, X. D. Zhu, R. R. Ullah, P. Klavins, and V. Taufour, J. Phys. Condens. Matter **35**, 045802 (2023).
[28] Q. H. Wang *et al.*, ACS Nano **16**, 6960 (2022).
[29] J.- X. Yin, B. Lian, and M. Zahid Hasan, Nature (London) **612**, 647 (2022).
[30] See Supplemental Material at http://link.aps.org/supplemental/10.1103/PhysRevB.108.L100408 for additional experimental results.
[31] R. Wolfe, R. D. Pierce, S. E. Haszko, and J. P. Remeika, Appl. Phys. Lett. **11**, 245 (1967).
[32] L. T. Tsymbal, G. N. Kakazei, and Ya. B. Bazaliy, Phys. Rev. B **79**, 092414 (2009).
[33] L. T. Tsymbal, Ya. B. Bazaliy, G. N. Kakazei, and S. V. Vasiliev, J. Appl. Phys. **108**, 083906 (2010).
[34] X. X. Ma, W. Fan, G. Zhao, H. Chen, C. Wang, B. Kang, Z. Feng, J.- Y. Ge, W. Ren, and S. Cao, Phys. Chem. Chem. Phys. **24**, 735 (2022).
[35] C. Kooy and U. Enz, Philips Res. Rep. **15**, 7 (1960).
[36] J. E. Davies, O. Hellwig, E. E. Fullerton, G. Denbeaux, J. B. Kortright, and K. Liu, Phys. Rev. B **70**, 224434 (2004).
[37] A. Noah, F. Toric, T. D. Feld, G. Zissman, A. Gutfreund, D. Tsruya, T. R. Devidas, H. Alpern, A. Vakahi, H. Steinberg, M. E. Huber, J. G. Analytis, S. Gazit, E. Lachman, and Y. Anahory, Phys. Rev. B **105**, 144423 (2022).
[38] S. Reich, S. Shtrikman, and D. Treves, J. Appl. Phys. **36**, 140 (1965).
[39] D. V. Ratnam and W. R. Buessem, J. Appl. Phys. **43**, 1291 (1972).
[40] Q. Wang, Y. Zeng, K. Yuan, Q. Zeng, P. Gu, X. Xu, H. Wang, Z. Han, K. Nomura, W. Wang, E. Liu, Y. Hou, and Y. Ye, Nat. Electron. **6**, 119 (2023).